Interlayer Charge Transfer and Photodetection Efficiency of Graphene–Transition-Metal-Dichalcogenide Heterostructures

Aparna Parappurath,[1,*,‡‡] Sreemanta Mitra,[1,†,§,‡‡] Gagandeep Singh,[1,¶] Navkiranjot Kaur Gill,[1] Tanweer Ahmed,[1,**] T. Phanindra Sai,[1] Kenji Watanabe,[2] Takashi Taniguchi,[3] and Arindam Ghosh[1,‡,††]

[1] *Department of Physics, Indian Institute of Science, Bangalore 560012, India*

[2] *Research Center for Functional Materials, National Institute of Materials Science, 1-1 Namiki, Tsukuba 305-0044, Japan*

[3] *International Center for Materials Nanoarchitectonics, National Institute of Materials Science, 1-1 Namiki, Tsukuba 305-0044, Japan*

(Received 29 November 2021; revised 13 May 2022; accepted 20 May 2022; published 30 June 2022)

Graphene and transition-metal-dichalcogenide- (TMD) based van der Waals heterostructures in field-effect-transistor (FET) architecture exhibits extremely high sensitivity to optical radiation due to transit and physical separation of the photogenerated carriers across the heterointerface. Both the sensitivity and speed of these detectors depend on the kinetics of charge transfer, but their interdependency at room temperature (T), where these detectors would be most useful, remains largely unexplored. Here we systematically measure the T dependence of the magnitude (gain) and timescale (bandwidth) of photoresponse in graphene-TMD heterostructures well up to the room T. The gain-bandwidth product is found to be strongly dependent on the power of optical illumination and increases with decreasing power (P), becoming as large as 1 MHz in the low-P limit. We find that thermally activated back transfer of charge from graphene to the TMD determines the response time of the detector at higher temperatures under continuous illumination. Our experiment reveals the impact of charge-transfer pathways on the performance in a broad class of graphene-TMD detectors.

DOI: 10.1103/PhysRevApplied.17.064062

I. INTRODUCTION

Since their inception, the superior light-matter interaction in two-dimensional (2D) materials and their van der Waals (vdW) heterostructure hybrids have been employed, not only to explore their possibilities in quantum technology applications but also to understand the conversion of light to electricity [1–16]. While the semiconducting 2D materials, which includes TMDs, showed promising outcomes in photodetector applications [17], their graphene-based vdW hybrids revolutionized the field with extremely high photoresponsivity (R^*) [18–22]. It is now well understood that the origin of such a large optical response is the high optical gain (G) whereby a single photon, which generates an electron-hole pair in the TMD layer produces many carriers in graphene, which acts as the channel of current flow [19]. Earlier work on the photoresponse of such graphene-based hybrid devices either explored on the origin of the photoresponse, ultrahigh R^* at low optical power (P), or the existence of gate-tunable persistent photoconductance, which may lead to optical-memory-device applications [19–22], including several studies for room-T broadband applications [23–25]. In contrast, systematic studies on the response time, or the bandwidth, of these detectors are comparatively few [26,27], which generally correlates the response time to the self-limiting rate of charge transfer from TMD to graphene upon optical illumination. Although these models provide a qualitative agreement with the experimentally observed response time [26], the role of back transfer of charge from the graphene to the TMD layer, which is likely to become increasingly

*aparnap@iisc.ac.in
†sreemanta85@gmail.com
‡arindam@iisc.ac.in
§Present address: Department of Physics, Gandhi Institute of Technology and Management (GITAM - Deemed to be University), Bangalore Campus, Dodballapura, Bangalore 561203, India.
¶Present address: Division of Physics and Applied Physics, Nanyang Technological University, Nanyang Link 637371, Singapore.
**Present address: CIC nanoGUNE BRTA, 20018 Donostia-San Sebastian, Basque Country, Spain.
††Also at Centre for Nano Science and Engineering, Indian Institute of Science, Bangalore 560012, India.
‡‡These authors contributed equally to the work.

 © 2022 American Physical Society

relevant with increasing T, remains largely unknown. Possibility of graphene → TMD charge transfer has been discussed in the context of sub-band gap photon absorption in pump-probe experiments [28,29] but their characteristics (e.g., dependence on temperature or optical P) in phototransistor architecture require further understanding.

If the TMD → graphene charge transfer is considered as the dominant process for photoresponse in these vdW hybrids, it is expected that the photoexcited electrons will be back to the TMD to recombine with the trapped holes, and the current in the channel reverts back to its initial dark-state value when the optical illumination is off. However, the observation of persistent photoconductivity, i.e., only partial recovery to the dark-state conductivity on turning the excitation off, indicates such recombination remains incomplete, especially at low temperatures ($T < 150$ K). It appears that there exists an energy barrier at the interface of the hybrids, that obstructs the return of the electrons back to the TMD, once the optical source is turned off. On the other hand, the vanishing persistent photoconductivity at room temperature implies that the evolution of photoresponse at the intermediate T is also useful to understand the photogenerated charge-carrier dynamics across the interface.

Here, we explore the effect of temperature on the photoconductivity of different TMD-based graphene vdW hybrid heterostructure devices. We observe that with increasing T, the probability of the photogenerated electrons moving back to the TMD and recombining with the localized holes increases in certain TMDs. This is experimentally manifested in the gradual decrease in the low-T persistent photoconductance with increasing T. Furthermore, our experiments suggest that the dynamics of photoresponse are crucially determined by the trap states in the TMD. Finally we have experimentally evaluated the gain-bandwidth (G-BW) product of our devices as a function of the optical power density P. Since both G and charge-transfer rate, i.e., BW, are determined by (1) P and (2) density of states in the graphene layer at the Fermi energy, they are strongly linked [26]. The inverse correlation between the gain ($G \sim 1/P$) and the device bandwidth (BW $\sim \tau_{\text{res}}^{-1} \sim P$), categorizes the 2D photodetectors broadly into two classes, either with high G and low temporal BW or vice versa. We find the G-BW product can be as large as 1 MHz, which compares very well with existing 2D-based detectors in the same P regime (approximately 100 fW/μm^2) of optical illumination.

II. DEVICE FABRICATION AND MEASUREMENTS

The graphene and few-layered TMD-based vdW heterostructure is created by layer-by-layer dry transfer [30] of mechanically exfoliated graphene and TMD. We use two different TMDs in this study, one being a six-layered thick WS_2 (dev A) and the other is a bilayer $MoSe_2$ (dev B) [31–34] to form the vertical heterostructures. The exfoliated flakes of graphene and TMD are then transferred onto a few-layered h-BN (exfoliated using the crystals from NIMS, Japan) flake on SiO_2/Si^{++} substrate, where the heavily doped p-type Si^{++} acts as a global back gate. The few-layered h-BN is a wide band gap (approximately equal to 6 eV) semiconductor, which acts as the bottom insulating surface with fewer defects than SiO_2 and also disregards the effect of defects at the SiO_2-TMD interface on the photoresponse. The TMD (WS_2 or $MoSe_2$) is covered with graphene, which acts as the measurement channel. The invasive electrical contacts are defined on graphene by e-beam lithography and made by subsequent metallization with thermally evaporated Cr (5 nm)/Au(50 nm). The optical images of the fabricated devices are shown in Fig. 1(a). The left panel shows the image of dev A and the right panel shows the image of dev B. The TMD and the graphene in dev B are larger than that of dev A. While the channel length in dev A is approximately equal to 1 μm, the same for dev B is 3 μm.

The devices are optically characterized prior to the electrical measurements, using the PL spectroscopy [Figs. 1(b) and 1(c)]. In Fig. 1(d), we show the typical device architecture schematic and the measurement scheme.

Electrical transport measurements are performed at high vacuum (pressure $\leq 10^{-5}$ mbar) inside a flow-type cryostat [20]. A Lake Shore temperature controller (LS331) is used to control and measure the temperature. We take a voltage-biased two-probe lock-in measurement technique for the majority of our transport experiments. In certain cases, we take a current-biased measurement approach as well. However, these two give no conflict to the understanding described. In the voltage bias measurements, a constant bias voltage (10 or 6 or 2.5 mV depending on the channel resistance, with a bias modulation frequency approximately equal to 217 Hz) is applied to the source (S) contact and the drain (D) current is measured using a lock-in amplifier (SR830) (time constant = 3 ms for the BW measurements, and 300 ms otherwise) on-board DAQ under optical illumination [yellow light-emitting diode (LED), 590 nm, 2.10 eV for dev A, and red LED, 635 nm, 1.95 eV for dev B]. The electrical pulses to drive the LED (Thor Labs) are mediated by the Stanford Research DS345 function synthesizer. The on and off time of the light pulses is created by Arbitrary Waveform Creator (AWC) software for DS345 with a modulation frequency of 1 kHz. A 2400 Keithley SMU is used to apply the back-gate voltage (V_{BG}). The current biased measurements, whenever conducted, are performed by applying a constant bias current (100 nA with a bias modulation frequency approximately equal to 217 Hz) and the voltage drop between the source and drain terminal is measured using the lock-in amplifier.

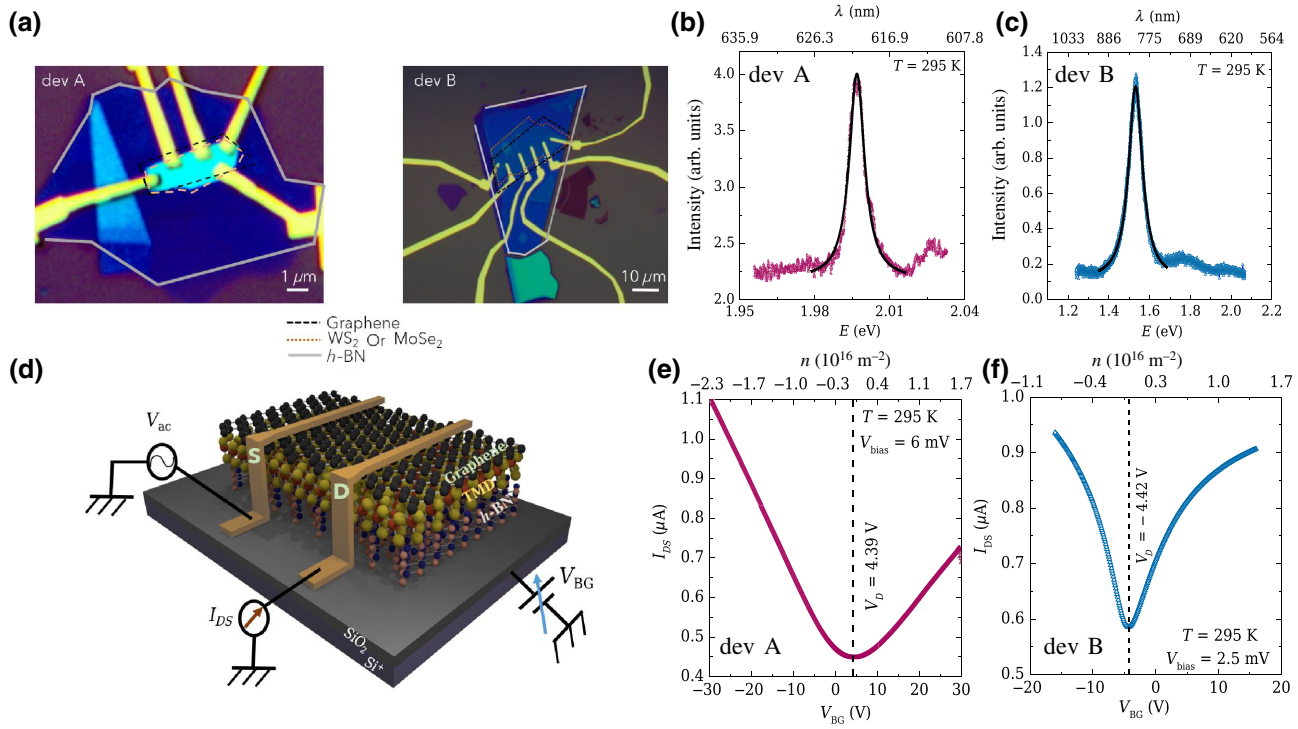

FIG. 1. Experimental consideration and primary characterizations of dev A (graphene/WS_2/*h*-BN) and dev B (graphene/$MoSe_2$/*h*-BN). (a) Optical image of dev A (graphene/WS_2/*h*-BN) and dev B (graphene/$MoSe_2$/*h*-BN). The channel length in dev A is approximately equal to 1 μm, and the same for dev B is 3 μm. (b) PL spectra of dev A, measured at 295 K. Excitonic contribution from WS_2 is observed at 1.996 eV ($\lambda = 621$ nm), with a linewidth of 73.4 meV. (c) Room temperature (295 K) PL spectra of dev B. The excitonic contribution from $MoSe_2$ is observed at 1.53 eV ($\lambda = 810.3$ nm), with a linewidth of 82.4 meV. The black solid lines in (b),(c) are the Lorentzian fit to the experimental data. (d) Illustration of the graphene-TMD device architecture and electrical measurement set up. A constant bias voltage is applied to the source (S) terminal, and drain (D) current (I_{DS}) is measured by a lock-in amplifier at diverse (including room) temperatures under various optical illumination conditions. The tunable dc voltage (V_{BG}) is applied to the p-doped Si^{++}, which acts as a global back gate. Room temperature (295 K) transfer characteristics (I_{DS}-V_{BG}) of (e) dev A, and (f) dev B. The minimum of current (I_{DS}) indicates the charge neutrality (or the Dirac point V_D) of dev A is 4.39 V and −4.42 V for dev B. The TMD starts conducting around 15 V and screens the applied V_{BG}, leading to a V_{BG} independent I_{DS}.

III. RESULTS AND DISCUSSIONS

We show the PL of the devices at 295 K in Figs. 1(b) and 1(c). The excitonic contribution for dev A [Fig. 1(b)] [35–37] is observed at 1.996 eV with a linewidth of 73.4 meV as evident from the Lorentzian fit (black solid line) to the experimental data. For dev B, as shown in Fig. 1(c), the excitonic peak appears at 1.53 eV with a line-width of 82.4 meV [38]. Excitonic peaks obtained from PL are also compared with values from optical absorption based experiments reported in the literature. We observe that the A excitonic peak (1.99 eV) for dev A is in agreement with the absorption data presented for five-layered WS_2 [39]. A similar comparison of the $MoSe_2$-based device (dev B) suggests the same [40]. The photoresponse of the device is obtained by illuminating photons with energy slightly greater than the optical band gap of the respective TMDs assuring nonzero optical density of states. Our previous work [21] showed that the photoresponse became maximum at the excitonic peak and remains almost constant for energies thereafter. Below the optical band gap, the photoresponse is greatly suppressed.

We begin to describe our transport data by showing the source-drain current (I_{DS}) in the graphene channel as a function of V_{BG} [Figs. 1(e) and 1(f) for dev A and dev B, respectively] in the dark state to understand their doping profile. For both devices, we observe the typical "bell-shaped" transfer characteristics of graphene on an insulating substrate. The charge neutrality point (V_D) at room temperature comes out to be 4.39 V (dev A) and −4.42 V (dev B), where I_{DS} become minimum. Being ambipolar, the graphene is hole doped for $V_{BG} < V_D$, while $V_{BG} > V_D$ indicates conduction by electron. The conduction threshold for the TMD, appears around 15 V [22,41] and for $V_{BG} > 15$ V, TMD starts conducting and screens the V_{BG} [22]. The carrier number density (n) in graphene is calculated using the parallel plate capacitor model described elsewhere [22].

A representative plot of the temporal dependence of I_{DS} for dev A under two successive optical pulses ($P = 1597$ fW/μm^2) measured at $T = 100$ K for $V_{BG} - V_D = -2$ V is presented in Fig. 2(a). Since V_D is T dependent (see Sec. II within the Supplemental Material [34]), we intend to show the T-dependent behavior at a particular $V_{BG} - V_D = -2$ V for a fair comparison. Figure 2(a) shows that I_{DS} for dev A changes by 3.9% and reduces to a lower value (I_{on}) under the optical illumination. This reduction of I_{DS} suggests a transfer of photoexcited electrons from WS_2 (TMD in general) to the hole-doped graphene [Fig. 2(b)] and reduced its carrier concentration by recombining with its holes. An opposite feature is observed for the electron-doped side of graphene, where the transferred electrons increase the carrier number density in graphene and I_{DS} increases under light (see Sec. III within the Supplemental Material [34]). The magnitude of the photocurrent (I_P) is defined as the difference between I_{off} and I_{on}. Once the first optical pulse is off, I_{DS} tends to go to the I_{off}, however, changes only by 0.9% and persists at I_{rec}. This again changes back to I_{on} on the arrival of a second optical pulse. A similar light-off trend is seen once the second pulse is turned off and a clear persistence at I_{rec} is observed (see Sec. IV within the Supplemental Material [34]). Similar behavior in dev B is also observed [Fig. 2(c)]. To reset the device and change I_{DS} back to I_{off}, a high V_{BG} sweep is applied [22].

As I_{DS} is both T and V_{BG} dependent as well, we calculate the net electron density (N_G)

$$N_G = \frac{1}{eC}\frac{I_P}{\frac{dI_{DS}}{dV_{BG}}}, \tag{1}$$

where C is the capacitance of the insulating gate barrier, transferred from TMD to graphene, that leads to I_P for the particular $V_{BG} - V_D$ following Ref. [21,22]. N_G follows a linear ($1/T$) dependence in a semilogarithmic representation for both the devices [Fig. 2(b) for dev A and

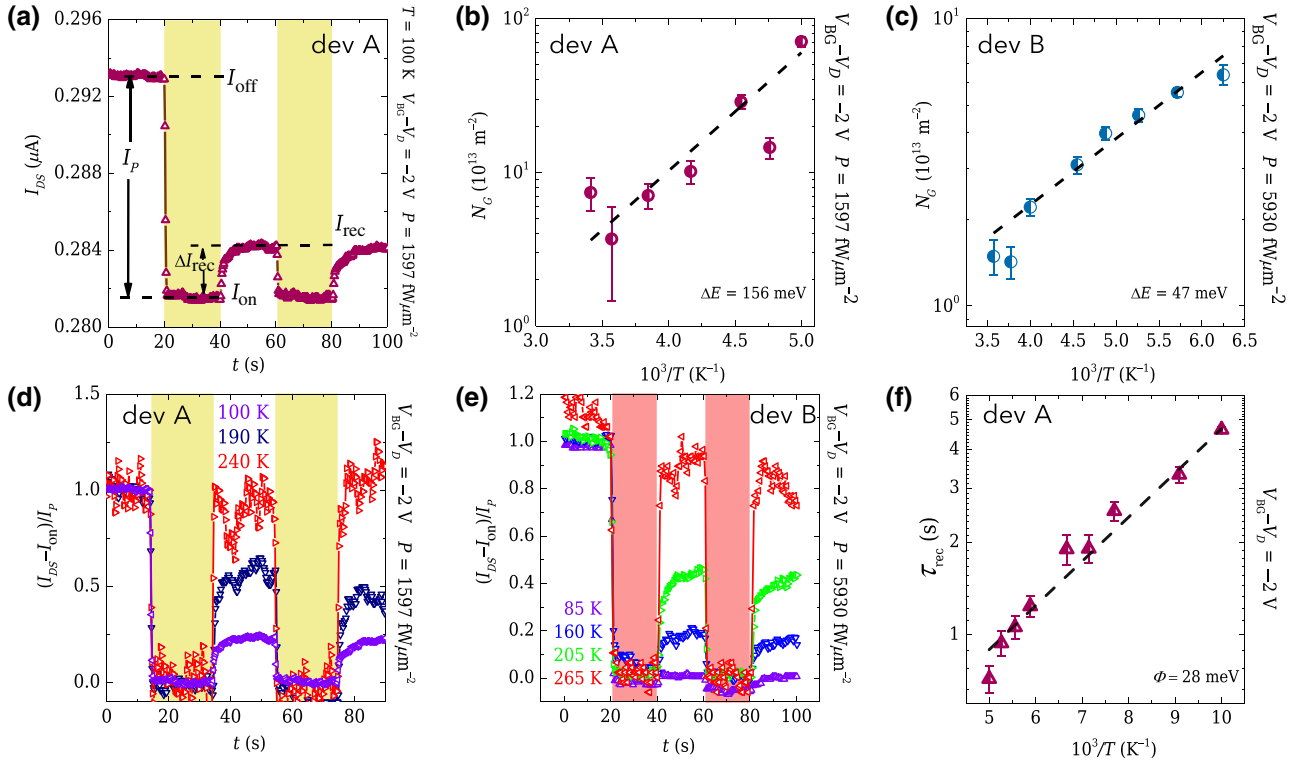

FIG. 2. Temperature dependence of the photoresponse. (a) $I_{DS} - t$ plot for dev A measured at $P = 1597$ fW/μm^2, $T = 100$ K, and $V_{BG} - V_D = -2$ V. I_P is the absolute photocurrent magnitude (defined as $I_{on} - I_{off}$, where I_{on} is the steady-state I_{DS} under illuminated condition and I_{off} is the dark current), I_{rec} is the steady state I_{DS}, after the optical pulse is turned off. ΔI_{rec} is the difference between I_{on} and I_{rec}. (b),(c) The T dependence of the net electron density (N_G) transferred to graphene from TMD. $N_G - T^{-1}$ followed a linear behavior in a semilogarithmic representation, suggesting an activated process. The black dashed line is the Arrhenius fit to elucidate the activation energy as 156 ± 34 meV (dev A) and 47 ± 4.6 meV (dev B). (d) Temporal dependence of normalized I_{DS} measured at $P = 1597$ fW/μm^2 and $V_{BG} - V_D = -2$ V for three different T for dev A. (e) Temporal dependence of normalized I_{DS} measured at $P = 5930$ fW/μm^2 and $V_{BG} - V_D = -2$ V for three different T for dev B. For both (d),(e) the increasing T increases I_{rec} and the persistence is gradually removed. (f) T dependence of recovery time (τ_{rec}) for dev A, measured at $V_{BG} - V_D = -2$ V. The decrease of τ_{rec} with increasing T, suggests electron back transfer is supported by the thermal energy ($k_B T$). The black dashed line is the Arrhenius fit to the experimental data to elucidate the activation energy (Φ), which comes out to be 28 ± 3.3 meV.

Fig. 2(c) for dev B], suggesting an activated process of the charge transfer associated. It is manifested in the reduction of I_P with increasing T [21]. An Arrhenius fit with

$$N_G \propto \exp\left(\frac{\Delta E}{k_B T}\right) \tag{2}$$

allows us to estimate the activation energy barrier (ΔE) as 156 ± 34 meV for dev A [Fig. 2(b)] and 47 ± 4.6 meV for dev B [Fig. 2(c)].

In Fig. 2(d), we show the temporal dependence of the normalized source-drain current ($(I_{DS} - I_{\text{off}})/I_P$) ($P = 1597$ fW/μm^2) for dev A measured at different T. Figure 2(e) shows a similar representative plot for dev B, measured with $P = 5930$ fW/μm^2. We observe the low-T persistence in photocurrent, gradually decreases with increasing T. Eventually, at higher T, persistence is completely subjugated and I_{DS} returns to I_{off}, without any external V_{BG} sweep, once the light is off.

While we find that the response time (τ_{res}) is independent of T (depends only on P [21,22,42,43]); interestingly, the recovery time (time taken by the device to go to the I_{rec}, τ_{rec}) decreases with increasing T. Figures 2(d) and 2(e) depict this behavior for both dev A and dev B, respectively. The increasing back-transfer rate (τ_{rec}^{-1}) with T, attests to the fact that the graphene $\longrightarrow$ TMD charge transfer is supported by the external thermal energy ($k_B T$), whereas, τ_{res}, associated with TMD $\longrightarrow$ graphene charge transfer is always energetically favorable due to the heterostructure band alignment, and, hence, remain T independent. We find that the τ_{rec} varies linearly with T^{-1} in a semilogarithmic representation [Fig. 2(f) for dev A measured at $V_{BG} - V_D = -2$ V], implying an Arrhenius-type activated process. The activation energy (Φ) comes out to be 28 ± 3.3 meV from the linear fit of the experimental data. The other device (dev B) also shows a similar behavior with respective Φ as 51 ± 3.8 meV (see Sec. V within the Supplemental Material [34]).

It may be convenient to explore the energy band diagram (Fig. 3) for this category of vdW hybrids to explain the photoresponse mechanism and the experimentally determined activation energies. Considering the conduction band edge of the TMD is at E_C, and the excitonic binding energy is E_b, the excitonic energy (E_X) in TMD appears at $E_C + E_b$. The work function of graphene (Dirac point, E_D) [44,45] allows us to estimate the position of the Fermi level (E_F) for any particular V_{BG} [45]. Together they form a type-II heterostructure, with a tunable energy difference ΔE at the interface determined by $E_X - E_F$, which leads to an effective charge separation at the interface. This holds for any graphene-semiconducting TMD-based hybrids [19,21,26]. For dev A, E_X of WS_2 lies around approximately equal to 110 meV above E_F for $V_{\text{BG}} - V_D = -2$ V, whereas for dev B, $E_X - E_F$ comes out to be approximately equal to 60 meV [34,46–52]. We observe that the calculated value of the $E_X - E_F$ agrees quite closely with the obtained activation energy from the $N_G - 1/T$ plot. This possibly implies that $E_X - E_F$ favors

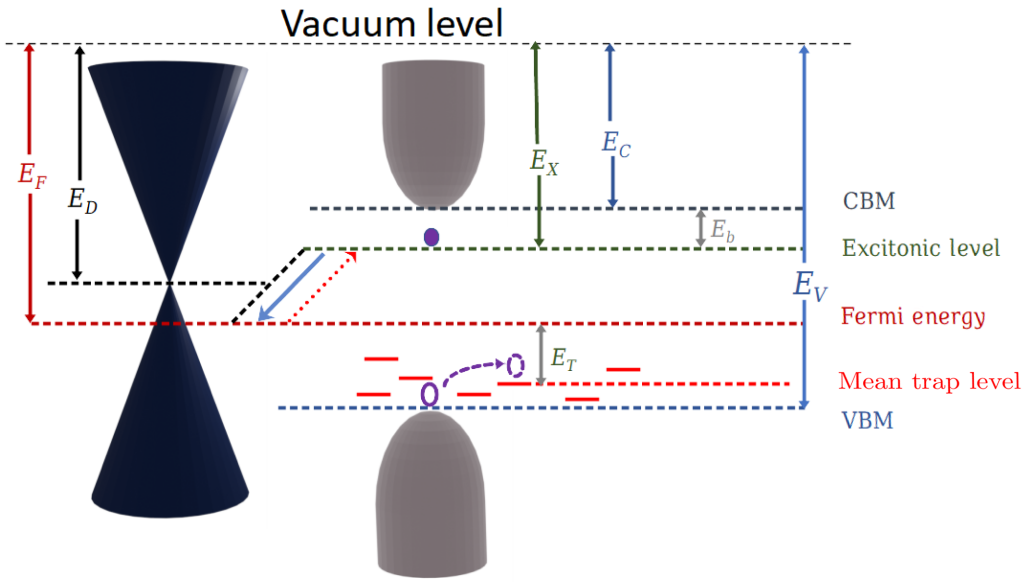

FIG. 3. Schematic of band alignment for graphene and TMD hybrid heterostructure. CBM and VBM represent the conduction band minima and the valance band maxima of the TMD, respectively. Alignment of bands at the interface favors electron transfer (represented with solid blue arrow) to graphene from TMD upon optical illumination. The back transfer of electron (red dotted arrow) is hindered by an energy barrier $E_X - E_F$. The optically generated electrons and holes are represented as filled and hollow violet circles respectively. The hole trap states are situated near VBM and their mean energy is away from the E_F by E_T. E_T is related to the detrapping energy of the holes.

the transfer of photoexcited electrons from E_X of TMD to E_F of graphene, however, the back transfer in the opposite direction is majorly restricted, due to the apparent energy barrier as appeared to the electrons in graphene.

At any instance of time, the effective I_{DS} is proportional to the difference between the number of electrons going into graphene (n^+) and coming back to TMD (n^-). At low-T, $n^+ \gg n^-$ leading to the persistence in I_P. The removal of persistent photoconductivity at higher temperatures implies that the number of photoexcited electrons that went into graphene and came back to TMD in the light-off condition, is comparable. The increasing T continues to provide extra thermal energy to the photoexcited electrons transferred to graphene and increase their probability to move back to the TMD and recombine with the trapped holes.

We believe that τ_{rec} is associated with the detrapping of the holes in the TMD. Detrapping times, in contrast to trapping times, depend strongly on the trap's energy level in the band gap [53]. The former will have an activated T-dependence, [53] and this activation energy is proportional to the energy gap between the Fermi level and the energy level of the hole trap (E_T). Quite possibly, the activation energy (Φ) from our $\tau_{\text{rec}} - (1/T)$ plot is related to this detrapping activation energy (E_T) and suggest that trap states in the TMD may lie a few meV away from the E_F.

We further note that there are possibilities of other relevant energy associated with this phenomenon. For example, the chalcogen atom vacancies in TMD create defect states near E_F, which trap these photoexcited holes are known to be localized [41,54–57]. For efficient recombination of the electrons and holes, this localization energy has to be overcome as well. Different TMDs in the devices cater defect states of different densities and the localization lengths of the holes are different as well. Alongside, this localization energy of the trap states will depend on the E_F (or V_{BG}). Hence, it will not be appropriate to compare quantitatively from different devices. However, the qualitative arguments hold true and this could be emphasized in the observation of persistent photoconductivity at room temperature in a similar device architecture with MoS_2 as the light-active element (see Sec. VII within the Supplemental Material [34]), where the localization energy is known to be significantly stronger [55] than WS_2 [41,56] or $MoSe_2$ [57]. Also the distribution of the midgap defect states and its manifestation at different T plays a key role in the photoresponse.

The observation of significant photoresponse at room temperature, allows us to explore the devices' optoelectronic characteristic features to be used as a room-temperature photodetector. The representative plots of the room-temperature photodetector application of dev A and dev B are shown in Figs. 4(a) and 4(b), respectively, where the temporal dependence of I_{DS} are shown for $V_{BG} = 0$ V (dev A) and $V_{BG} = -8$ V (dev B) with nine 200 ms optical pulses of P, viz., 16 800 fW/μm^2 (for dev A) and 64 930 fW/μm^2 (for dev B). As the optical pulse is on, I_{DS} decreases by 0.8% from I_{off} and moves to a lower level, I_{on} and comes back to I_{off} when the pulse goes off without showing any persistence. It thus replicates the light on-off pulse and, hence can be used as a good photodetector. The on:off ratio is 0.99 and is found to be weakly dependent on P. The high dark current appears due to the highly conducting graphene as the channel material [58]. At $V_{\text{BG}} = 0$ V (dev A) or $V_{BG} = -8$ V (dev B) the graphene is hole doped [see Fig. 1(e) for dev A and Fig. 1(f) for dev B] and this decrease of I_{DS} under optical illumination is consistent with the photoresponse mechanism based on TMD to graphene charge transfer discussed earlier [19–22]. The similar room-temperature response from both the devices indicates that the previously discussed charge-transfer mechanism for low T applies at room temperature as well. The magnitude of I_P [Fig. 4(c)] comes out to be 6.35 nA for the highest P used and decreases only by a small factor. For the two P, differing by order of magnitude, I_P changes only by 0.2%. The apparent P independence of I_P gives rise to a significantly large responsivity (R^*) at low P in this type of binary hybrid [19,21,22].

The high-frequency photoswitching measurements are required to estimate photodetector response time (τ_{res}), which is defined as the time for I_{DS} to reach from $0.1I_P$ to $0.9I_P$. The limiting number of τ_{res} is used to define the maximum operating frequency as [17]

$$f = \frac{1}{(2\pi\,\tau_{\text{res}})_{\text{max}}}. \tag{3}$$

In Fig. 4(d), we show the way we determine the room temperature τ_{res} for dev A measured at $V_{BG} = 0$ V with 16 800 fW/μm^2. τ_{res} comes out to be 14.9 ms, giving rise to a bandwidth (BW, defined as $0.35/\tau_{\text{res}}$) [59] of 23.5 Hz. A similar estimation gives the BW of dev B as 35 Hz (see Sec. VIII within the Supplemental Material [34]). Although τ_{res} is P dependent, [21,22,42,43], it become almost P independent at the current experimental P window and limited by the measurement electronics (see Sec. IX within the Supplemental Material [34]).

The frequency dependence of the photocurrent measured under square pulse light modulation [Fig. 5(a)] shows that the photocurrent begins to decrease beyond a characteristic roll over frequency $f_0 = 10$ Hz corresponding to a characteristic transient time $\tau_0 = (2\pi f_0)^{-1} =$ 16 ms [9]. Following the bandwidth convention, the characteristic time constant ($\tau_{3\text{ dB}} = (2\pi f_{3\text{ dB}})^{-1}$) comes out to be 7.5 ms. Our current measuring amplifier (lock in) is characterized by the time constant of 3 ms. This implies that our BW estimation is limited by the capacitive time constant of the instrument electronics, as also observed

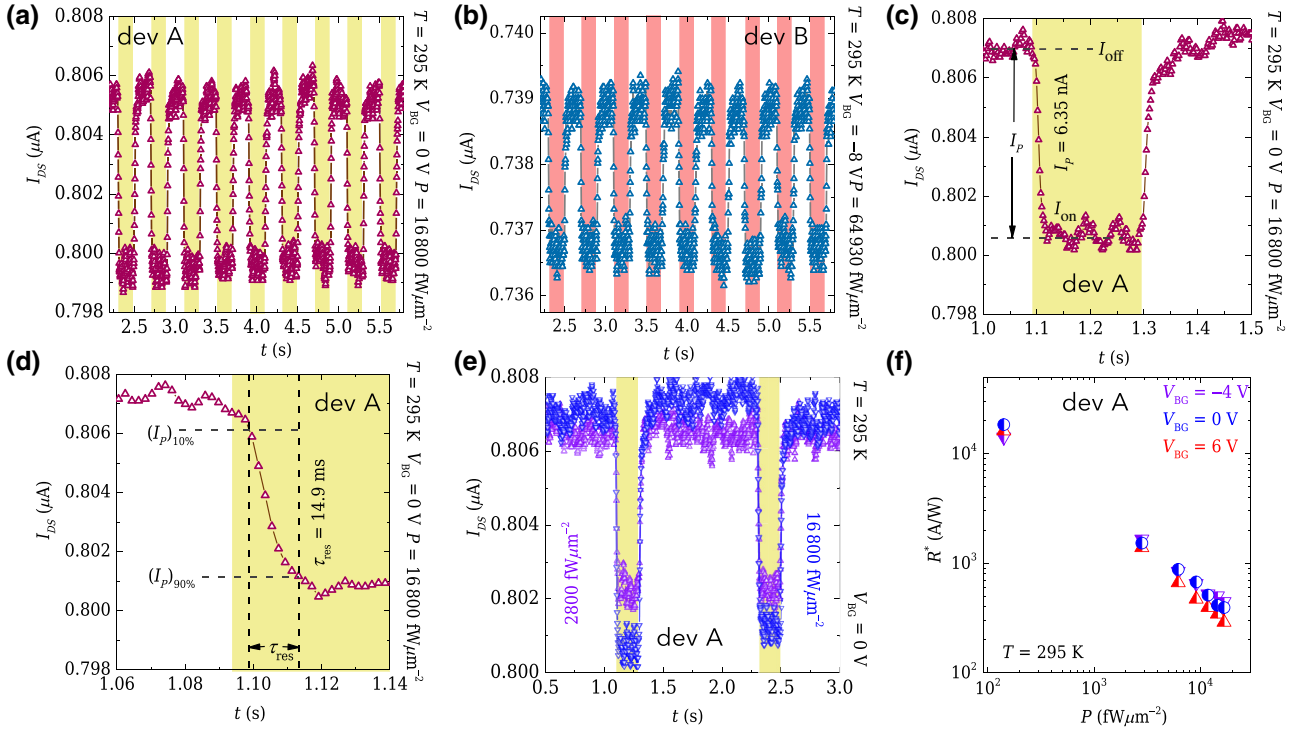

FIG. 4. Room-temperature photoresponse of graphene/TMD/h-BN hybrid devices. $I_{DS} - t$ plots measured at room temperature, for (a) WS_2-based device (dev A) with 16 800 fW/μm^2 and (b) $MoSe_2$ based device (dev B) with 64 900 fW/μm^2. Nine input optical pulses with 200 ms on and off time are used as input (590 nm for dev A and 635 nm for dev B) to describe their utility in photodetector applications. These optical pulses are also used to determine the speed of the devices to elucidate their bandwidth. (c) A representation of room temperature I_{DS}-t for a 200 ms optical pulse (P = 16 800 fW/μm^2) measured at V_{BG} = 0 V to elucidate the magnitude of photocurrent (I_P). (d) Enlarged plot of (a) to determine the response time (τ_{res}) of the device. τ_{res} is defined as the time taken to go from 10% I_P to 90% I_P. At 16 800 fW/μm^2, τ_{res} comes out to be 14.9 ms. (e) Temporal (t) dependence of I_{DS} under two 200 ms optical pulses separated by 1 s. The two plots are of different optical power density, viz., 16 800 fW/μm^2 (blue) and 2800 fW/μm^2 (violet). Under the optical illumination, I_{DS} decreases from its dark-state value, implying an increase in device resistance. The measurements are done at 295 K and 0 V V_{BG}. The I_P is decreased slightly by an order of magnitude change in P, leading to a significantly high photoresponsivity ($R^* \approx 10^4$ A/W) at low power. (f) The variation of responsivity (R^*) with P. R^* increases as P is decreased and reaches to 10^4 A/W at the lowest P used. This value of R^* gives rise to a photoconductive gain of 10^5.

previously (Refs. [9,60,61] and Sec. X within the Supplemental Material [34]) and the interlayer charge-transfer time, which gives the τ_{res}, is much faster (approximately of the order of a few ps) as evident from the pump-probe experiments in this type of hybrid device [62]. Nonetheless, it is worth noting that the estimated τ_{res} in our devices are comparable to the other FET-based photodetectors [5,17,63].

At room temperature, τ_{rec} is approximately equal to 30 ms. This limits the device resetting time (dead time) and thus if two pulses come in a timescale shorter than this dead time, the device will not distinguish them as two separate pulses.

In Fig. 4(e), we show the temporal response of I_{DS} of dev A for a two 200 ms pulses separated by 1 s. R^*, one of the useful figures of merit for photodetectors, defines the number of excess carriers collected in the external circuit for incident unit power and depends on both P and incident wavelength (λ), and is found to be as high as 10^4 A/W for dev A [Fig. 4(f)]. A slightly lower R^* (approximately equal to 5×10^2 A/W) appears for dev B, possibly due to the larger device area and comparatively higher P of the light source used.

At our lowest P, the photoconductive gain (G) is calculated to be 10^5 (for dev A) and 10^3 (for dev B), following [22]

$$G = \frac{hcR^*}{e\lambda\eta}, \tag{4}$$

where h, c, e, λ, η are Planck's constant, velocity of light in vacuum, electronic charge, excitation wavelength, and internal quantum efficiency (estimated as 0.3 for various TMD photodetectors) [26]. G follows a similar P dependence as R^* for both dev A and dev B (see Sec. IX within the Supplemental Material [34]).

The high R^* (or G) and the reasonably high BW of these devices give rise to another trade of art, G-BW product,

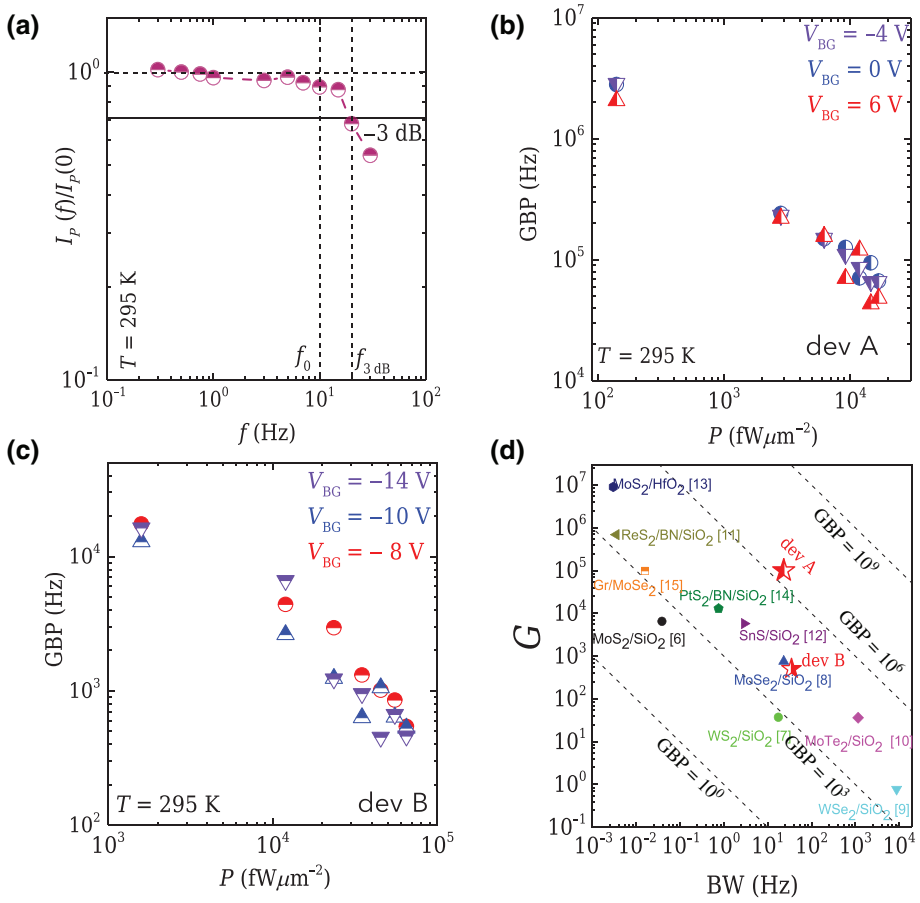

FIG. 5. Optical power (P) dependence of GBP at room temperature and the state of the art. (a) LED modulation frequency dependence of the normalized photocurrent. The photocurrent starts to decrease from the zero-frequency value near 10 Hz and eventually reduced by 3 dB at 20 Hz, which determines the BW. P dependence of the G-BW product (GBP) for dev A (b) and dev B (c) measured at room temperature for three different V_{BG}. The GBP is independent of V_{BG} and goes to a high value of 1 MHz (dev A) and 10 kHz (dev B) for the lowest of the applied P. (d) The current status of the TMD and its hybrid-based FET photodetectors in the G-BW phase space. Our devices, dev A and dev B, are marked in red, and stands high in comparison to the other similar phototransistors.

which appears to be higher than several other FET photodetectors [17]. Since the BW is largely independent of P in its current experimental window (see Sec. IX within the Supplemental Material [34]), GBP increases with decreasing P in a manner similar to that of R^* [19,21,22] and reaches to a value approximately equal to 1 MHz for dev A [Fig. 5(b)] and 10 kHz for dev B [Fig. 5(c)]. The P dependence of GBP for both the devices appear to be independent of V_{BG} [Figs. 5(b) and 5(c)]. In Fig. 5(d), we intend to show the current status of TMD and its hybrid-based FET photodetectors in the G-BW phase space at room temperature. With G of 10^5 and BW of 23.5 Hz, dev A stands well above many of its contemporary devices, while dev B with a G of 10^3 and BW of 35 Hz shows promising possibility. These two devices' photoresponse characteristics suggests that graphene and TMD-hybrid-heterostructure FET devices have the quality to be considered as one of the efficient FET photodetectors at room temperature, alongside being contemplated as an optical memory device at low T.

For the photodetector applications, several characteristic parameters need to be computed based on G and BW, and two out of them are the noise equivalent power (NEP) and the specific detectivity (D^*) (see Sec. XI within the Supplemental Material [34]). NEP ($= \sqrt{S_t}/R^*$) measures the minimum detectable power of I_P above the noise floor where

$$S_t = S_{\text{th}} + S_{\text{sh}} + S_f \tag{5}$$

is the spectral density of noise and its estimation is crucial and should be performed experimentally under different operating conditions [17]. The Johnson noise (S_{th}) is given by $4k_BT/R_{\text{dark}}$ with k_B is the Boltzmann constant, and R_{dark} is the dark-state resistance of the phototransistor. S_{sh} is the shot noise, and is given by $2eI_{DS}$ under the dark state. While S_{sh} and S_{th} are frequency independent, S_f is the low-frequency $1/f$ noise. Considering the BW of these devices as 20 Hz, S_f comes around 10^{-22} A^2/Hz [26], while

S_{th} and S_{sh} are approximately around 10^{-24} A^2/Hz and 10^{-25} A^2/Hz, respectively. Similarly, the specific detectivity ($D^* = \sqrt{A}/\text{NEP}$) indicates the minimum detectable power per unit area (A) of the device and unity BW and useful for cross-platform performance comparison. At the lowest P, of 100 fW/μm^2, NEP comes out to be 10^{-16} W/Hz$^{1/2}$ (see Ref. [34] for a detailed calculation of the NEP), which leads to a high value of D^*($\approx 10^{12}$ Jones) where A is approximately equal to 1 μm^2.

IV. SUMMARY

In summary, we made a systematic T-dependent study of the optoelectronic properties of the graphene-TMD vdW hybrid FETs to explore the possibility to tune their optoelectronic response and understand the device characteristics at room temperature. We find that the signature low-T persistent photoconductivity of these hybrid FETs is removed by thermal energy, which helps the photogenerated transferred electrons from graphene to come back to the TMD and recombine at a higher T. We find while the response time is P dependent, its T independence suggests that the graphene to TMD charge transfer under the optical illumination is energetically favorable. We describe that the bidirectional charge-transfer probability could be tuned with thermal energy. Furthermore, the temperature variation of the recovery time suggests that the charge-transfer probability also depends on the position of the trap states in the TMD. We find that the low-T photogating mechanism prevails at room temperature as well. Our measurements elucidate the instrument-limited response time of these FET devices, which suggests a higher BW compared to many of its contemporaries, along with significant gain. The high GBP for our devices attest to our claim of graphene and TMD FET to be one of the most efficient photodetectors at room temperature.

DATA AVAILABILITY

The data that support the findings of this study are available from the corresponding author on reasonable request.

ACKNOWLEDGMENTS

The authors acknowledge financial support from U.S. Army International Technology Centre Pacific (ITC-PAC) and Ministry of Electronic and Information Technology (MEITy), Govt. of India. A.P. and S.M. would like to acknowledge Dr. Saloni Kakkar Kakkar for fruitful discussions. A.P. thanks Ministry of Education, Govt. of India for the Prime Minister's Research Fellowship (PMRF). S.M. thanks University Grants Commission (UGC) India for the financial support as Dr. D.S. Kothari Post Doctoral Fellowship (DSKPDF grant number F.4-2/2006 (BSR)/PH/19-20/0094). K.W. and T.T. acknowledge support from JSPS KAKENHI (Grants No. 19H05790, No. 20H00354, and No. 21H05233).

A.G. envisioned the project and supervised it. A.P. and S.M. designed the project with A.G. and have contributed equally to this work. A.P. and S.M. performed the transport and opto-electronic measurements and analysed the subsequent data. G.D.S., N.K.G., T.P.S., and T.A. have contributed in fabrication, basic optical-characterization and measurement-set-up processes. K.W. and T.T. grew the h-BN crystals. A.P. and S.M. drafted the manuscript with input from all authors. All the authors have gone through the paper and declare no competing financial interests.

[1] Victor W. Brar, Michelle C. Sherrott, and Deep Jariwala, Emerging photonic architectures in two-dimensional opto-electronics, Chem. Soc. Rev. **47**, 6824 (2018).

[2] F. H. L. Koppens, T. Mueller, Ph. Avouris, A. C. Ferrari, M. S. Vitiello, and M. Polini, Photodetectors based on graphene, other two-dimensional materials and hybrid systems, Nat. Nanotechnol. **9**, 780 (2014).

[3] G. Konstantatos, Current status and technological prospect of photodetectors based on two-dimensional materials, Nat. Commun. **9**, 5266 (2018).

[4] Yi-Feng Xiong, Jin-Hui Chen, Yan-Qing Lu, and Fei Xu, Broadband optical-fiber-compatible photodetector based on a graphene-MoS_2-WS_2 heterostructure with a synergetic photogenerating mechanism, Adv. Electr. Mater. **5**, 1800562 (2019).

[5] Wenzhi Yu, Shaojuan Li, Yupeng Zhang, Weiliang Ma, Tian Sun, Jian Yuan, Kai Fu, and Qiaoliang Bao, Near-infrared photodetectors based on $MoTe_2$/graphene heterostructure with high responsivity and flexibility, Small **13**, 1700268 (2017).

[6] O. Lopez-Sanchez, D. Lembke, M. Kayci, A. Radenovic, and A. Kis, Ultrasensitive photodetectors based on monolayer MoS_2, Nat. Nanotechnol. **8**, 497 (2013).

[7] Nengjie Huo, Shengxue Yang, Zhongming Wei, Shu-Shen Li, Jian-Bai Xia, and Jingbo Li, Photoresponsive and gas sensing field-effect transistors based on multilayer WS_2 nanoflakes, Sci. Rep. **4**, 1 (2014).

[8] A. Abderrahmane, P. J. Ko, T. V. Thu, S. Ishizawa, T. Takamura, and A. Sandhu, High photosensitivity few-layered $MoSe_2$ back-gated field-effect phototransistors, Nanotechnology **25**, 365202 (2014).

[9] Nihar R. Pradhan, Jonathan Ludwig, Zhengguang Lu, Daniel Rhodes, Michael M. Bishop, Komalavalli Thirunavukkuarasu, Stephen A. McGill, Dmitry Smirnov, and Luis Balicas, High photoresponsivity and short photoresponse times in few-layered WSe_2 transistors, ACS Appl. Mater. Interfaces **7**, 12080 (2015).

[10] Tobias J. Octon, V. Karthik Nagareddy, Saverio Russo, Monica F. Craciun, and C. David Wright, Fast high-responsivity few-layer $MoTe_2$ photodetectors, Adv. Opt. Mater. **4**, 1750 (2016).

[11] Erfu Liu, Mingsheng Long, Junwen Zeng, Wei Luo, Yaojia Wang, Yiming Pan, Wei Zhou, Baigeng Wang, Weida

Hu, and Zhenhua Ni, *et al.*, High responsivity phototransistors based on few-layer ReS_2 for weak signal detection, Adv. Funct. Mater. **26**, 1938 (2016).

[12] Vaishnavi Krishnamurthi, Hareem Khan, Taimur Ahmed, Ali Zavabeti, Sherif Abdulkader Tawfik, Shubhendra Kumar Jain, Michelle J. S. Spencer, Sivacarendran Balendhran, Kenneth B. Crozier, and Ziyuan Li, *et al.*, Liquid-metal synthesized ultrathin sns layers for high-performance broadband photodetectors, Adv. Mater. **32**, 2004247 (2020).

[13] Roda Nur, Takashi Tsuchiya, Kasidit Toprasertpong, Kazuya Terabe, Shinichi Takagi, and Mitsuru Takenaka, High responsivity in MoS_2 phototransistors based on charge trapping HfO_2 dielectrics, Commun. Mater. **1**, 1 (2020).

[14] Liang Li, Weike Wang, Yang Chai, Huiqiao Li, Mingliang Tian, and Tianyou Zhai, Few-layered PtS_2 phototransistor on h-BN with high gain, Adv. Funct. Mater. **27**, 1701011 (2017).

[15] Beiyun Liu, Congya You, Chen Zhao, Gaoliang Shen, Yawei Liu, Yufo Li, Hui Yan, and Yongzhe Zhang, High responsivity and near-infrared photodetector based on graphene/$MoSe_2$ heterostructure, Chin. Opt. Lett. **17**, 020002 (2019).

[16] Sreemanta Mitra, Divya Srivastava, Shib Shankar Singha, Saurav Dutta, Biswarup Satpati, Maarit Karppinen, Arindam Ghosh, and Achintya Singha, Tailoring phonon modes of few-layered MoS_2 by in-plane electric field, npj 2D Mater. Appl. **4**, 6 (2020).

[17] Kartikey Thakar and Saurabh Lodha, Optoelectronic and photonic devices based on transition metal dichalcogenides, Mater. Res. Express **7**, 014002 (2020).

[18] L. Britnell, R. M. Ribeiro, A. Eckmann, R. Jalil, B. D. Belle, A. Mishchenko, Y.-J. Kim, R. V. Gorbachev, T. Georgiou, S. V. Morozov, A. N. Grigorenko, A. K. Geim, C. Casiraghi, A. H. Castro Neto, and K. S. Novoselov, Strong light-matter interactions in heterostructures of atomically thin films, Science **340**, 1311 (2013).

[19] Kallol Roy, Medini Padmanabhan, Srijit Goswami, T. Phanindra Sai, Gopalakrishnan Ramalingam, Srinivasan Raghavan, and Arindam Ghosh, Graphene–MoS_2 hybrid structures for multifunctional photoresponsive memory devices, Nat. Nanotechnol. **8**, 826 (2013).

[20] Kallol Roy, Tanweer Ahmed, Harshit Dubey, T. Phanindra Sai, Ranjit Kashid, Shruti Maliakal, Kimberly Hsieh, Saquib Shamim, and Arindam Ghosh, Number-resolved single-photon detection with ultralow noise van der Waals hybrid, Adv. Mater. **30**, 1704412 (2018).

[21] Ranjit Kashid, Jayanta Kumar Mishra, Avradip Pradhan, Tanweer Ahmed, Saloni Kakkar, Pranav Mundada, Preeti Deshpande, Kallol Roy, Ambarish Ghosh, and Arindam Ghosh, Observation of inter-layer charge transmission resonance at optically excited graphene-tmdc interfaces, APL Mater. **8**, 091114 (2020).

[22] Sreemanta Mitra, Saloni Kakkar, Tanweer Ahmed, and Arindam Ghosh, Graphene-WS_2 van der Waals Hybrid Heterostructure for Photodetector and Memory Device Applications, Phys. Rev. Appl. **14**, 064029 (2020).

[23] Wenjie Deng, Yongfeng Chen, Congya You, Boxing An, Beiyun Liu, Songyu Li, Yongzhe Zhang, Hui Yan, and Ling Sun, Visible-infrared dual-mode MoS_2-graphene-MoS_2 phototransistor with high ratio of the I_{ph}/I_{dark}, 2D Mater. **5**, 045027 (2018).

[24] Domenico De Fazio, Ilya Goykhman, Duhee Yoon, Matteo Bruna, Anna Eiden, Silvia Milana, Ugo Sassi, Matteo Barbone, Dumitru Dumcenco, Kolyo Marinov, Andras Kis, and Andrea C. Ferrari, High responsivity, large-area graphene/MoS_2 flexible photodetectors, ACS Nano **10**, 8252 (2016).

[25] Shan Gao, Ziqian Wang, Huide Wang, Fanxu Meng, Pengfei Wang, Si Chen, Yonghong Zeng, Jinlai Zhao, Haiguo Hu, Rui Cao, Zhongquan Xu, Zhinan Guo, and Han Zhang, Graphene/MoS_2/graphene vertical heterostructure-based broadband photodetector with high performance, Adv. Mater. Interfaces **8**, 2001730 (2021).

[26] Tanweer Ahmed, Kallol Roy, Saloni Kakkar, Avradip Pradhan, and Arindam Ghosh, Interplay of charge transfer and disorder in optoelectronic response in graphene/hBN/MoS_2 van der waals heterostructures, 2D Mater. **7**, 025043 (2020).

[27] Vinh X. Ho, Yifei Wang, Michael P. Cooney, and N. Q. Vinh, Graphene-Ta_2O_5 heterostructure enabled high performance, deep-ultraviolet to mid-infrared photodetection, Nanoscale **13**, 10526 (2021).

[28] Shuai Fu, Indy du Fossé, Xiaoyu Jia, Jingyin Xu, Xiaoqing Yu, Heng Zhang, Wenhao Zheng, Sven Krasel, Zongping Chen, and Zhiming M. Wang, *et al.*, Long-lived charge separation following pump-wavelength-dependent ultrafast charge transfer in graphene/WS_2 heterostructures, Sci. Adv. **7**, eabd9061 (2021).

[29] Long Yuan, Ting-Fung Chung, Agnieszka Kuc, Yan Wan, Yang Xu, Yong P. Chen, Thomas Heine, and Libai Huang, Photocarrier generation from interlayer charge-transfer transitions in WS_2-graphene heterostructures, Sci. Adv. **4**, e1700324 (2018).

[30] Sidi Fan, Quoc An Vu, Minh Dao Tran, Subash Adhikari, and Young Hee Lee, Transfer assembly for two-dimensional van der Waals heterostructures, 2D Mater. **7**, 022005 (2020).

[31] Juhong Park, Min Su Kim, Eunho Cha, Jeongyong Kim, and Wonbong Choi, Synthesis of uniform single layer WS_2 for tunable photoluminescence, Sci. Rep. **7**, 16121 (2017).

[32] Yuanzheng Li, Xinshu Li, Tong Yu, Guochun Yang, Heyu Chen, Cen Zhang, Qiushi Feng, Jiangang Ma, Weizhen Liu, Haiyang Xu, Yichun Liu, and Xinfeng Liu, Accurate identification of layer number for few-layer WS_2 and WSe_2 via spectroscopic study, Nanotechnology **29**, 124001 (2018).

[33] Philipp Tonndorf, Robert Schmidt, Philipp Böttger, Xiao Zhang, Janna Börner, Andreas Liebig, Manfred Albrecht, Christian Kloc, Ovidiu Gordan, Dietrich R. T. Zahn, Steffen Michaelis de Vasconcellos, and Rudolf Bratschitsch, Photoluminescence emission and raman response of monolayer MoS_2, $MoSe_2$, and WSe_2, Opt. Express **21**, 4908 (2013).

[34] See Supplemental Material at http://link.aps.org/supplemental/10.1103/PhysRevApplied.17.064062 for AFM and Raman spectroscopy of the devices (Sec. I), temperature dependence of charge neutrality point v_D (Sec. II), photoresposne in electron-doped graphene (Sec. III), long light-off time response of the device at low temperature (Sec. IV), t dependence of recovery time for dev B (Sec. V), the

calculation of energy scales (Sec. VI), room-temperature persistent photoconductivity for the MoS_2-based device (Sec. VII), response time for dev B (Sec. VIII), variation of gain-bandwidth product with power (Sec. IX), effect of measurement electronics (Sec. X), and calculation of noise equivalent power (Sec. XI).

[35] M. Currie, A. T. Hanbicki, G. Kioseoglou, and B. T. Jonker, Optical control of charged exciton states in tungsten disulfide, Appl. Phys. Lett. **106**, 201907 (2015).

[36] Weijie Zhao, Zohreh Ghorannevis, Leiqiang Chu, Minglin Toh, Christian Kloc, Ping-Heng Tan, and Goki Eda, Evolution of electronic structure in atomically thin sheets of WS_2 and WSe_2, ACS Nano **7**, 791 (2013).

[37] Tara Shankar Bhattacharya, Sreemanta Mitra, Shib Shankar Singha, Prasanna Kumar Mondal, and Achintya Singha, Tailoring light-matter interaction in WS_2-gold nanoparticles hybrid systems, Phys. Rev. B **100**, 235438 (2019).

[38] Arelo O. A. Tanoh, Jack Alexander-Webber, Ye Fan, Nicholas Gauriot, James Xiao, Raj Pandya, Zhaojun Li, Stephan Hofmann, and Akshay Rao, Giant photoluminescence enhancement in $MoSe_2$ monolayers treated with oleic acid ligands, Nanoscale Adv. **3**, 4216 (2021).

[39] Weijie Zhao, Zohreh Ghorannevis, Leiqiang Chu, Minglin Toh, Christian Kloc, Ping-Heng Tan, and Goki Eda, Evolution of electronic structure in atomically thin sheets of WS_2 and WSe_2, ACS Nano **7**, 791 (2013).

[40] Ningning Dong, Yuanxin Li, Yanyan Feng, Saifeng Zhang, Xiaoyan Zhang, Chunxia Chang, Jintai Fan, Long Zhang, and Jun Wang, Optical limiting and theoretical modelling of layered transition metal dichalcogenide nanosheets, Sci. Rep. **5**, 1 (2015).

[41] Dmitry Ovchinnikov, Adrien Allain, Ying-Sheng Huang, Dumitru Dumcenco, and Andras Kis, Electrical transport properties of single-layer WS_2, ACS Nano **8**, 8174 (2014).

[42] Dominik Kufer and Gerasimos Konstantatos, Highly sensitive, encapsulated MoS_2 photodetector with gate controllable gain and speed, Nano Lett. **15**, 7307 (2015).

[43] Marco M. Furchi, Dmitry K. Polyushkin, Andreas Pospischil, and Thomas Mueller, Mechanisms of photoconductivity in atomically thin MoS_2, Nano Lett. **14**, 6165 (2014).

[44] Rusen Yan, Qin Zhang, Wei Li, Irene Calizo, Tian Shen, Curt A. Richter, Angela R. Hight-Walker, Xuelei Liang, Alan Seabaugh, Debdeep Jena, Huili Grace Xing, David J. Gundlach, and N. V. Nguyen, Determination of graphene work function and graphene-insulator-semiconductor band alignment by internal photoemission spectroscopy, Appl. Phys. Lett. **101**, 022105 (2012).

[45] Young-Jun Yu, Yue Zhao, Sunmin Ryu, Louis E. Brus, Kwang S Kim, and Philip Kim, Tuning the graphene work function by electric field effect, Nano Lett. **9**, 3430 (2009).

[46] Pil Ju Ko, Abdelkader Abderrahmane, Nam-Hoon Kim, and Adarsh Sandhu, High-performance near-infrared photodetector based on nano-layered $MoSe_2$, Semicond. Sci. Technol. **32**, 065015 (2017).

[47] Han-gyu Kim and Hyoung Joon Choi, Thickness dependence of work function, ionization energy, and electron affinity of Mo and W dichalcogenides from DFT and GW calculations, Phys. Rev. B **103**, 085404 (2021).

[48] Garima Gupta, Sangeeth Kallatt, and Kausik Majumdar, Direct observation of giant binding energy modulation of exciton complexes in monolayer $MoSe_2$, Phys. Rev. B **96**, 081403 (2017).

[49] M. Goryca, Jing Li, Andreas V. Stier, Takashi Taniguchi, K. Watanabe, Emmanuel Courtade, S. Shree, Cedric Robert, B. Urbaszek, and X. Marie, *et al.*, Revealing exciton masses and dielectric properties of monolayer semiconductors with high magnetic fields, Nat. Commun. **10**, 1 (2019).

[50] Filip A. Rasmussen and Kristian S. Thygesen, Computational 2D materials database: Electronic structure of transition-metal dichalcogenides and oxides, J. Phys. Chem. C **119**, 13169 (2015).

[51] Ziliang Ye, Ting Cao, Kevin O'brien, Hanyu Zhu, Xiaobo Yin, Yuan Wang, Steven G. Louie, and Xiang Zhang, Probing excitonic dark states in single-layer tungsten disulphide, Nature **513**, 214 (2014).

[52] Bairen Zhu, Xi Chen, and Xiaodong Cui, Exciton binding energy of monolayer WS_2, Sci. Rep. **5**, 1 (2015).

[53] G. Kramberger, V. Cindro, I. Mandić, M. Mikuž, and M. Zavrtanik, Determination of detrapping times in semiconductor detectors, J. Instrum. **7**, P04006 (2012).

[54] Subhamoy Ghatak, Atindra Nath Pal, and Arindam Ghosh, Nature of electronic states in atomically thin MoS_2 field-effect transistors, ACS Nano **5**, 7707 (2011).

[55] Kallol Roy, Medini Padmanabhan, Srijit Goswami, T. Phanindra Sai, Sanjeev Kaushal, and Arindam Ghosh, Optically active heterostructures of graphene and ultrathin MoS2, Solid State Commun. **175-176**, 35 (2013). Special Issue: Graphene V: Recent Advances in Studies of Graphene and Graphene Analogues.

[56] Nikos Papadopoulos, Pascal Gehring, Kenji Watanabe, Takashi Taniguchi, Herre S. J. Van Der Zant, and Gary A. Steele, Tunneling spectroscopy of localized states of WS_2 barriers in vertical van der Waals heterostructures, Phys. Rev. B **101**, 165303 (2020).

[57] Dhavala Suri and R. S. Patel, Electron and thermal transport via variable range hopping in $MoSe_2$ single crystals, Appl. Phys. Lett. **110**, 233108 (2017).

[58] Shaili Sett, Aparna Parappurath, Navkiranjot Kaur Gill, Neha Chauhan, and Arindam Ghosh, Engineering sensitivity and spectral range of photodetection in van der Waals materials and hybrids, Nano Express **3**, 014001 (2022).

[59] D. Descoster and J. Harari, *Optoelectronic Sensors* (John Wiley & Sons, London, 2009), 284.

[60] Atiye Pezeshki, Seyed Hossein Hosseini Shokouh, Tavakol Nazari, Kyunghwan Oh, and Seongil Im, Electric and photovoltaic behavior of a few-layer α-$MoTe_2$/MoS_2 dichalcogenide heterojunction, Adv. Mater. **28**, 3216 (2016).

[61] Vinod K. Sangwan, Joohoon Kang, David Lam, J. Tyler Gish, Spencer A. Wells, Jan Luxa, James P. Male, G. Jeffrey Snyder, Zdeněk Sofer, and Mark C. Hersam, Intrinsic carrier multiplication in layered Bi_2O_2Se avalanche photodiodes with gain bandwidth product exceeding 1 GHz, Nano Res. **14**, 1961 (2021).

[62] Long Yuan, Ting-Fung Chung, Agnieszka Kuc, Yan Wan, Yang Xu, Yong P. Chen, Thomas Heine, and Libai Huang, Photocarrier generation from interlayer charge-transfer transitions in WS_2-graphene heterostructures, Sci. Adv. **4**, e1700324 (2018).

[63] Chao-Hui Yeh, Hsiang-Chieh Chen, Ho-Chun Lin, Yung-Chang Lin, Zheng-Yong Liang, Mei-Yin Chou, Kazu Suenaga, and Po-Wen Chiu, Ultrafast monolayer In/Gr-WS_2-Gr hybrid photodetectors with high gain, ACS Nano **13**, 3269 (2019).